Inorganic Chemistry
Article

Inorg. Chem. **2009**, *48*, 6261–6270 **6261**
DOI: 10.1021/ic900573w

$EuTM_2Ga_8$ (TM = Co, Rh, Ir) — A Contribution to the Chemistry of the $CeFe_2Al_8$-type Compounds

O. Sichevych,[†,‡] M. Kohout,[†] W. Schnelle,[†] H. Borrmann,[†] R. Cardoso-Gil,[†] M. Schmidt,[†] U. Burkhardt,[†] and Yu. Grin*[,†]

[†] *Max-Planck-Institut fur Chemische Physik fester Stoffe, Nothnitzer Str. 40, 01187 Dresden, Germany, and* [‡] *Department of Chemistry, National University of Forestry and Wood Technology of Ukraine, General Chuprynka Str. 103, 79013 Lviv, Ukraine*

Received March 24, 2009

The isostructural compounds $EuTM_2Ga_8$ (TM = Co, Rh, Ir) were prepared by direct reaction of the elements by high-frequency thermal treatment. All three phases are isotypic with $CeFe_2Al_8$ (space group *Pbam*, Pearson symbol *oP*44, $Z = 4$). The crystal structure was established from single-crystal X-ray diffraction data: $a = 12.4322(7)$ Å, $b = 14.3814(9)$ Å, and $c = 4.0378(2)$ Å for $EuCo_2Ga_8$; $a = 12.6001(6)$ Å, $b = 14.6757(7)$ Å, and $c = 4.1172(2)$ Å for $EuRh_2Ga_8$; and $a = 12.6237(7)$ Å, $b = 14.6978(8)$ Å, and $c = 4.1486(2)$ Å for $EuIr_2Ga_8$, respectively. Analysis of the chemical bonding in $EuRh_2Ga_8$ with the electron localizability tools reveals formation of the 3D $[Rh_2Ga_8]$ polyanion build by polar covalent bonds. Europium interacts in two ways with the polyanion: mainly as a cation by charge transfer and additionally covalently by means of the electrons of the inner shells. Magnetic susceptibility measurements show Curie−Weiss paramagnetic behavior above 40 K with effective magnetic moments of 7.81, 8.05, and 8.27 μ_B/f.u. for $EuTM_2Ga_8$ (TM = Co, Rh, Ir). Antiferromagnetic ordering of Eu moments is observed in all three compounds below 20 K. Independently on the chemical composition of the coordination sphere, magnetic behavior and, especially, X-ray absorption spectra indicate predominantly the $4f^7$ electronic configuration of europium with small admixture of the $4f^6$ state.

1. Introduction

Gallium-rich compounds of rare-earth and transition metals have attracted strong attention since the discovery of a wide variety of physical phenomena in the $RCoGa_5$ phases (R = U, rare-earth metals).[1−5] The observation of the superconductivity in the heavy-fermion material $CeRhGa_5$[6,7] extended the interest from gallium-containing systems to the phases of gallium's analogues, indium and aluminum. The investigated phase diagrams of the ternary systems R−TM−{Al,Ga}, where TM is a transition metal, reveal that often several other structural patterns are in competition with that of the $HoCoGa_5$-type one.[8,9] Especially for the light rare-earth or alkaline-earth metals as divalent cations, the $HoCoGa_5$-type structure is not stable any more. Instead of or in addition to that, another structural pattern appears, mostly that of the $CeFe_2Al_8$ type.[10] Attempts to prepare the $RTME_5$ phases led to the discovery of the compounds $EuRh_2E_8$ (E = Ga, In).[11] In the present work, we report on a new representative of the $CeFe_2Al_8$ type — the ternary compound $EuIr_2Ga_8$ — and discuss the crystal chemistry and chemical bonding of $EuTM_2Ga_8$ compounds (TM = Co, Rh, Ir) and their physical properties in comparison with other phases with the crystal structure of the $CeFe_2Al_8$ type.

Several series of compounds with the $CeFe_2Al_8$-type crystal structure have been observed for E = Al, Ga, and In: RFe_2Al_8 (R = La, Ce, Pr, Eu),[10,12,13] RCo_2Al_8 (R = Ca,

*To whom correspondence should be addressed. Tel.: +49-351-46464000. E-mail: grin@cpfs.mpg.de.

(1) Grin, Yu; Yarmoljuk, Ya. P; Gladyshevskii, E. I. *Sov. Phys. Crystallogr.* **1979**, *24*, 137–139.
(2) Grin, Yu.; Rogl, P.; Hiebl, K. *J. Less-Common Met.* **1986**, *121*, 497–505.
(3) Hudis, J.; Hu, R.; Broholm, C. L.; Mitrovic, V. F.; Petrovic, C. *J. Magn. Magn. Mater.* **2006**, *307*, 301–307.
(4) Matsuda, T. D.; Haga, Y.; Sakai, H.; Aoki, D.; Ikeda, S.; Yamamoto, E.; Shihido, H.; Settai, R.; Harima, H.; Onuki, Y. *J. Phys. Soc. Jpn.* **2008**, *77*, 024704.
(5) Noguchi, S.; Okuda, K. *J. Magn. Magn. Mater.* **1992**, *104*, 57–59.
(6) Hegger, H.; Petrovic, C.; Moshopoulou, E. G.; Hundley, M. F.; Sarrao, J. L.; Fisk, Z.; Thompson, J. D. *Phys. Rev. Lett.* **2000**, *84*, 4986–4989.
(7) Moshopoulou, E. G.; Fisk, Z.; Sarrao, J. L.; Thomson, J. D. *J. Solid State Chem.* **2001**, *158*, 25–33.
(8) Grin, Yu., Gladyshevskii, R. Gallides. *Metallurgia*; Moscow **1989**.
(9) Villars, P.; Prince, A.; Okamoto, H. *Handbook of Ternary Alloys Phase Diagrams*; ASM: Materials Park, OH, **1995**.
(10) Yarmolyuk, Ya. P.; Rychal, R. M.; Zarechnyuk, O. S. *Second All-Union Conf. on the Crystal Chemistry of Intermetallic Compounds, Book of Abstracts*; Lviv, Ukraine, **1974**; p 39.
(11) Fritsch, V.; Bobev, S.; Moreno, N. O.; Fisk, Z.; Thompson, J. D.; Sarrao, J. L. *Phys. Rev.* **2004**, *B70*, 052410.

Published on Web 05/26/2009

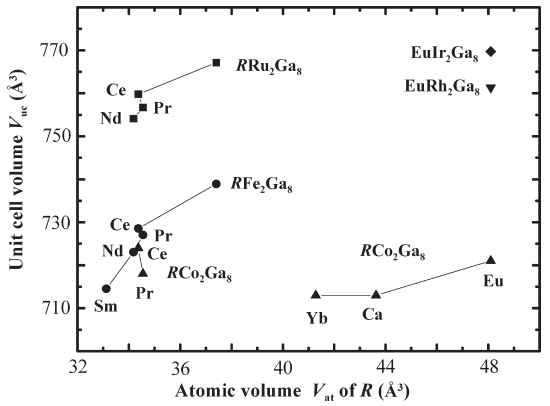

Figure 1. Unit cell volume of the RTM_2Ga_8 compounds versus atomic volume of the R component.

Ce, Pr, Sm, Yb),[14−17] RNi_2Al_8 (R = Ca),[18] $YbNi_{1.09}Fe_{0.91}Al_8$,[19] RFe_2Ga_8 (R = La, Ce, Pr, Nd, Sm),[20] RCo_2Ga_8 (R = Ca, Ce, Pr, Eu, Yb),[8,20,21] RRu_2Ga_8 (R = La−Nd),[22] RRh_2Ga_8 (R = Eu),[11,23] RIr_2Ga_8 (R = Eu),[23] and RRh_2In_8 (R = Sr, Eu).[24,25] The unit cell volumes for RTM_2Ga_8 compounds are summarized in Figure 1 in comparison with the atomic volumes of the R component obtained from the elemental crystal structures of the rare-earth metals stable under ambient conditions. The unit cell volume of the RTM_2E_8 compounds follows the size of the TM component (volumes of the Ru compounds are larger that those of the iron compounds, similarly to the observation made for the europium representatives with cobalt, rhodium, and iridium). In each series RTM_2E_8, the volume of the unit cell increases with the increasing atomic volume of R, with the exception of the cerium compounds. From this analysis, the volume behavior of the RTM_2Ga_8 compounds is similar to that of the R elements, suggesting a similar electronic configuration of the rare-earth (and alkaline-earth) metals in the RTM_2Ga_8 phases (excepting the $CeTM_2Ga_8$ compounds) and in the elements.

On the other hand, two phases with similar composition — $Eu_2Rh_3Ga_9$ and $Eu_2Ir_3Ga_9$ — were found recently.[26] Small admixtures of the $4f^6$ in addition to the majority $4f^7$ state for Eu were observed for these compounds from the magnetic susceptibility measurements and the X-ray absorption spectroscopy investigations. The experimental origin for admixtures from the oxidation products of the intermetallic compounds during the experiment was excluded as far it was possible but without assurance because of the known problems with the possible amorphous character of the oxidation products. The intrinsic reason may be the chemical interaction between europium and the more electronegative components like rhodium or iridium. In case of $Eu_2TM_3Ga_9$ compounds, a direct interaction of this kind was hard to detect: the Eu−TM distances in the crystal structure are on the order of 4 Å.

Thus, the $EuTM_2Ga_8$ compounds with the shortest Eu−TM distances of ca. 3.5 Å are suitable objects not only for the crystal chemical studies of the structure type $CeFe_2Al_8$, but also for the next step of investigations of the chemical interaction between the rare-earth metals and their environment in the ternary intermetallic compounds and the influence of the environment of the valence state of the R component.

2. Experimental Section

2.1. Preparation. Starting materials for the preparation of $EuCo_2Ga_8$, $EuRh_2Ga_8$, and $EuIr_2Ga_8$ were ingots of europium (Johnson Matthey or Lamprecht, stated purity 99.9%), cobalt foil (ChemPur, 99.9%), rhodium and iridium foils (ChemPur, 99.9%), and gallium lumps (ChemPur, 99.9999%). Europium was redistilled in a vacuum prior use.

For the preparation of $EuCo_2Ga_8$, and $EuRh_2Ga_8$ pieces of the elemental components were mixed in stoichiometric ratios and reacted in carbon crucibles in a high-frequency furnace under an argon atmosphere. For the synthesis of $EuIr_2Ga_8$, pieces of the iridium and gallium were prereacted to form $IrGa_3$ to increase the reactivity of the iridium-containing educt. Then, $IrGa_3$, gallium, and europium were reacted to obtain $EuIr_2Ga_8$ in glassy carbon crucibles by high-frequency treatment under an argon atmosphere.

Single crystals of $EuIr_2Ga_8$ were obtained by melting of the components in a sealed tantalum tube under an argon pressure of about 800 mbar (at room temperature). The tantalum tube was subsequently enclosed in an evacuated silica ampule. The ampule was heated to 1200 °C within 20 h and held at this temperature for 2 h. After that, the temperature was slowly (50 °C/h) reduced to 600 °C. The sample was annealed at this temperature for 14 days and subsequently quenched in cold water. Both synthetic routes (open glassy carbon and closed tantalum container techniques) lead to a single-phase product of $EuIr_2Ga_8$, as can be concluded from X-ray powder diffraction and metallographic analysis.

2.2. Characterization. The samples were characterized by X-ray powder diffraction using an Imaging Plate Guinier Camera (Huber G670, Co Kα1 radiation, λ = 1.788965 Å). Unit cell parameters were refined by a least-squares procedure using the peak positions extracted from powder patterns measured with LaB_6 as an internal standard (a = 4.15692 Å). Indexing of the diffraction peaks in the powder diagrams was controlled by intensity calculations using atomic parameters from the refined crystal structures. All crystallographic calculations were performed with the program package WinCSD.[27]

Metallographic analysis was performed on the annealed samples by using light optical microscopy (Zeiss Axioplan 2)

(12) Manjako, N. B.; Stec′, I. N.; Kavich, J. V.; Zarechnjuk, O. S.; Janson, T. I. *Dopov. Akad. Nauk Ukr. RSR Ser. B: Geol. Khim. Biol. Nauki* **1983**, *6*, 41–45.
(13) Klesnar, H.; Rogl, P. *J. Mater. Res.* **1991**, *6*, 53–56.
(14) Czech, E.; Cordier, G.; Schafer, H. *J. Less-Common Met.* **1983**, *95*, 205–211.
(15) Zarechnjuk, O. S.; Rykhal′, R. M.; Korin′, V. V. *Dopov. Akad. Nauk Ukr. RSR Ser. A: Fiz.-Mat. Techn. Nauki* **1980**, *1*, 86–89.
(16) Rykhal′, R. M.; Zarechnjuk, O. S.; Protasov, V. C. *Dopov. Akad. Nauk Ukr. RSR Ser. A: Fiz-Mat. Techn. Nauki* **1985**, *12*, 73–75.
(17) Manjako, N. B.; Janson, T. I.; Bodak, O. I.; Cerny, R.; Yvon, K. *Z. Kristallogr.* **1996**, *211*, 216.
(18) Manjako, N. B.; Janson, T. I.; Zarechnjuk, O. S. *Izv. Akad. Nauk SSSR Metally* **1988**, *3*, 185–189.
(19) Wu, X.; Francisco, M.; Rak, Z.; Bakas, T.; Mahanti, S. D.; Kanatzidis, M. G. *J. Solid State Chem.* **2008**, *181*, 3269–3277.
(20) Sichevych, O. M.; Lapunova, R. V.; Grin, Yu.; Yarmolujk, Ya. P. *Izv. Akad. Nauk SSSR Metally* **1985**, *6*, 117–118.
(21) Gladyshevskii, R. E.; Yarmolujk, Ya. P.; Grin, Yu. *Sov. Phys. Crystallogr.* **1983**, *28*, 841–843.
(22) Schluter, M.; Jeitschko, W. *Inorg. Chem.* **2001**, *40*, 6362–6368.
(23) Sichevych, O.; Schnelle, W.; Bormann, H.; Cardoso-Gil, R.; Schmidt, M.; Burkhardt, U.; Grin, Yu. *Absracts of the International Conference on Crystal Chemistry of Intermetallic Compounds*; Lviv, Ukraine, **2007**; p 137.
(24) Muts, I. R.; Zaremba, V. I.; Pottgen, R.; Anorg, Z. *Allg. Chem.* **2007**, *633*, 2234–2237.
(25) Pottgen, R.; Kussmann, D.; Anorg, Z. *Allg. Chem.* **2001**, *627*, 55–60.
(26) Sichevych, O.; Schnelle, W.; Prots, Yu.; Burkhardt, U.; Grin, Yu. *Z. Naturforsch.* **2006**, *61b*, 904–911.
(27) Akselrud, L. G.; Zavalii, P. Y.; Grin, Yu.; Pecharsky, V.; Baumgartner, B.; Wolfel, E. *Mater. Sci. Forum* **1993**, *133−136*, 335–340.

Table 1. Crystallographic Data and Crystal Structure Refinement Parameters of $EuCo_2Ga_8$, $EuRh_2Ga_8$, and $EuIr_2Ga_8$ (Space group *Pbam,* Pearson symbol *oP44*, $Z = 4$)

compound	$EuCo_2Ga_8$	$EuRh_2Ga_8$	$EuIr_2Ga_8$
a, Å[a]	12.4322(7)	12.6001(6)	12.6237(7)
b, Å	14.3814(9)	14.6757(7)	14.6978(8)
c, Å	4.0378(2)	4.1172(2)	4.1486(2)
a/c; b/c	3.079; 3.562	3.060; 3.564	3.042; 3.543
unit cell volume, Å^3	721.9(1)	761.3(1)	769.7(1)
D_{calcd}, g cm^{-3}	7.61	7.99	9.44
absorption coefficient, cm^{-1}	440.45	414.53	734.72
radiation; wavelength, Å	Ag Kα; 0.56087	Mo Kα; 0.71073	Mo Kα; 0.71073
diffractometer	STOE IPDS	STOE STADI 4	Rigaku AFC7/CCD
refinement mode	$F(hkl)$	$F(hkl)$	$F(hkl)$
cutoff	$F(hkl) > 6\sigma(F)$	$F(hkl) > 4\sigma(F)$	$F(hkl) > 4\sigma(F)$
$2\theta_{max}$	56	50	65
$N(hkl)$ measured	12787	3202	7798
$N(hkl)$ unique	1856	1169	1169
$R(F)$	0.049	0.048	0.036

[a] The lattice parameters were obtained from Guinier X-ray powder diffraction data.

as well as scanning electron microscopy (SEM, Philipps XL 30). The polished ingots were prepared under inert conditions in an argon-filled glovebox in the special setup.[28] Silicon carbide paper was used for grinding and diamond polishing, with at least 1/4 μm diamond powder applied for polishing. The microstructure surface was cleaned in a hexane bath with paraffin oil, which acts as a lubricant for the preparation of microstructures.

Magnetic susceptibility in external fields $\mu_0 H$ of 0.01, 0.1, and 1 T was determined in the temperature range 1.8−400 K in a SQUID magnetometer (MPMS XL-7, Quantum Design) on polycrystalline samples. Magnetization isotherms were taken at 1.8 K for fields up to $\mu_0 H = 7$ T.

The Eu-L_{III} X-ray absorption spectra (XAS) of polycrystalline $EuCo_2Ga_8$, $EuRh_2Ga_8$, and $EuIr_2Ga_8$ were recorded in a transmission arrangement at the EXAFS II beamline E4 of HASYLAB at DESY. Wavelength selection was realized by means of a Si(111) double-crystal monochromator, which yields an experimental resolution of approximately 2 eV (fwhm) for the experimental step at the Eu-L_{III} threshold of 6977 eV. The powdered samples were mixed with boron carbide and located in a special sample holder with beryllium windows for protecting the samples against air and moisture. This operation was performed in an argon-filled glovebox. The data were measured using Eu_2O_3 as an external reference for energy calibration. Deconvolution of the XAS spectra was performed with the program XasWin.[29]

2.3. Crystal Structure Determination. The quality of the single crystals was checked by precession and Laue photographs. The intensity data sets were collected from the qualitatively best single crystals: $EuCo_2Ga_8$ on a STOE IPDS setup (graphite monochromator, Ag Kα radiation, $\lambda = 0.56087$ Å), $EuRh_2Ga_8$ on a STOE STADI 4 (Mo Kα radiation, $\lambda = 0.71073$ Å), and $EuIr_2Ga_8$ on a Rigaku AFC7 diffractometer equipped with a Mercury CCD detector using Mo Kα radiation, $\lambda = 0.71073$ Å. Crystallographic information and experimental details are shown in Table 1.

2.4. Calculation Procedures. Electronic structure calculations and bonding analysis were carried out for $EuRh_2Ga_8$ using the TB-LMTO-ASA program package.[30] The von Barth−Hedin exchange potential[31] was employed for the LDA calculations. The radial scalar-relativistic Dirac equation was solved to get the partial waves. Because the calculation within the atomic sphere approximation (ASA) includes corrections for the neglect of interstitial regions and partial waves of higher order,[32] an addition of empty spheres was not necessary. The following radii of the atomic spheres were applied for the calculations: r(Eu) = 2.110 Å, r(Rh1) = 1.434 Å, r(Rh2) = 1.462 Å, r(Ga1) = 1.593 Å, r(Ga2) = 1.410 Å, r(Ga3) = 1.469 Å, r(Ga4) = 1.395 Å, r(Ga5) = 1.596 Å, r(Ga6) = 1.593 Å, r(Ga7) = 1.560 Å, r(Ga8) = 1.566 Å, r(Ga9) = 1.668 Å. A basis set containing Eu(6s,5d,4f), Ga(4s,4p), and Rh(5s,5p,4d) orbitals was employed for a self-consistent calculation with Eu (6p), Ga(3d), and Rh(4f) functions being downfolded. Spin-polarized calculation was performed.

The electron localizability indicator (ELI, Y)[33] was evaluated in the ELI-D representation according to refs 34 and 35 with an ELI-D module within the TB-LMTO-ASA[30] program packages. The procedure for calculation of the partial ELI-D contributions from different energy ranges in electronic DOS was implemented in the TB-LMTO-ASA code. For the isolated Eu atom, a relativistic ZORA calculation was performed with the ADF code[36] using the TZ2P basis set.

ELI-D and electron density were analyzed using the program Basin[37] with consecutive integration of the electron density in basins, which are bound by zero-flux surfaces in the ELI-D or electron density gradient field. Such treatment of ELI-D is similar to the procedure proposed by Bader for the electron density.[38]

3. Results and Discussion

3.1. Homogeneity Ranges. For the precise determination of the mutual homogeneity range of the RTM_2Ga_8 phases in the phase diagrams R−TM−Ga, the samples with the excess of gallium or TM (compared with the ideal composition $Eu_9TM_{18}Ga_{73}$, at. %) were prepared on the isoconcentrates of Eu. All prepared samples contained more than one phase: $Eu_9Co_{20}Ga_{71}$ ($EuCo_2Ga_8$ + CoGa + $EuGa_2$), $Eu_9Co_{16}Ga_{75}$ ($EuCo_2Ga_8$ + $EuGa_4$), $Eu_9Rh_{20}Ga_{71}$ ($EuRh_2Ga_8$ + $Eu_2Rh_3Ga_9$), $Eu_9Ga_{16}Ga_{75}$ ($EuRh_2Ga_8$ + $Eu_2Rh_3Ga_9$ + $EuGa_4$), $Eu_9Ir_{20}Ga_{71}$

(28) Schnelle, W.; Burkhardt, U.; Ramlau, R.; Niewa, R.; Sparn, G. *Scientific Report*; MPI CPfS: Dresden, Germany, **2003**; pp 38−40.
(29) Akselrud, L. G.; Grin, Yu. *XasWin*; Max-Planck-Institut fur Chemische Physik fester Stoffe: Dresden, Germany, **2004**.
(30) Jepsen, O.; Burkhardt, A.; Andersen, O. K. *The Program TB-LMTO-ASA*, version 4.7; Max-Planck-Institut fur Festkorperforschung: Stuttgart, Germany, **1999**.
(31) von Barth, U.; Hedin, L. *J. Phys. (Paris)* **1972**, *C5*, 1629–1642.
(32) Andersen, O. K. *Phys. Rev.* **1975**, *B12*, 3060–3083.
(33) Kohout, M. *Int. J. Quantum Chem.* **2004**, *97*, 651–658.
(34) Kohout, M.; Wagner, F. R.; Grin, Yu. *Int. J. Quantum Chem.* **2006**, *106*, 1499–1507.
(35) Kohout, M. *Faraday Disscuss.* **2007**, *135*, 43–54.
(36) *ADF 2007.01*, SCM, Vrije Universiteit: Amsterdam, The Netherlands, **2007**.
(37) Kohout, M. *Basin*, version 4.3; Max-Planck-Institut fur Chemische Physik fester Stoffe: Dresden, Germany, **2008**.
(38) Bader, R. F. W. *Atoms in Molecules: A Quantum Theory*; Oxford University Press: Oxford, U.K., **1999**.

($EuIr_2Ga_8$ + $Eu_2Ir_3Ga_9$), and $Eu_9Ir_{16}Ga_{75}$ ($EuIr_2Ga_8$ + $EuGa_4$). The lattice parameters of the $EuTM_2Ga_8$ phases in the multiphase samples were, within one or two estimated standard deviations, equal to that of the single-phase samples (Table 1). Both observations reveal clearly the "line-compound" character of all three phases (negligible homogeneity ranges).

The microstructure of the samples with (WDXS detected) compositions $Eu_{9.09(2)}Co_{18.18(2)}Ga_{72.73(3)}$, $Eu_{9.09(1)}Rh_{18.18(2)}Ga_{72.73(3)}$, and $Eu_{9.09(2)}Ir_{18.18(2)}Ga_{72.73(1)}$ is formed mainly by the target compounds $EuCo_2Ga_8$, $EuRh_2Ga_8$, and $EuIr_2Ga_8$, respectively (Figure 2). Only traces of minority phases were observed on the grain boundaries of the majority phase: $EuGa_4$ and CoGa in the cobalt-containing sample, $Eu_2Rh_3Ga_9$ in the rhodium-containing sample, and $Eu_2Ir_3Ga_9$ and $Eu_{18.3}Ir_{2.6}Ga_{79}$ in the iridium-containing sample.

3.2. Crystal Structure. Irregularly shaped crystals of $EuCo_2Ga_8$, $EuRh_2Ga_8$, and $EuIr_2Ga_8$ were isolated from the annealed samples. The starting atomic parameters were obtained from direct methods. The crystal structures were successfully refined with anisotropic displacement parameters for all atoms. For interatomic distance calculations, lattice parameters obtained from Guinier powder diffraction data were used. Final atomic coordinates and displacement parameters are given in Table 2; related interatomic distances are listed in Table 3.

There are 12 crystallographically unique positions in the $EuTM_2Ga_8$ structure — one for Eu, two for TM, and nine for Ga (Table 3). All atoms are situated on mirror planes at $z = 0$ and $z = 1/2$ (Figure 3). The Eu atoms' centered pentagonal prisms were formed by the 10 nearest Ga atoms at distances from 3.108(3) Å (Co), 3.138(3) Å (Rh), and 3.1345(9) Å (Ir) to 3.186(3) Å (Co), 3.206(3) Å (Rh), and 3.2197(9) Å (Ir). The five rectangular faces of the [Ga_{10}] prisms are capped by five other Ga atoms at distances ranging from 3.181(5) Å (Co), 3.232(5) Å (Rh), and 3.221(1) Å (Ir) to 3.953(5) Å (Co), 4.046(4) Å (Rh), and 4.051(1) Å (Ir). Both TM positions are situated in tricapped trigonal prisms formed by gallium atoms (CN = 9). However, the TM2 atom has an additional TM2 ligand at distance of 2.786(6) Å (Co), 2.969(4) Å (Rh), and 2.9898(5) Å (Ir).

The shortest distances between Rh and Ga atoms (< 2.50 Å, cf. Table 3) are markedly shorter than the sum of atomic (metallic) radii of Rh (1.345 Å[39]) and Ga (1.41 Å), being rather closer to the sum of covalent radii (1.25 Å for both, Rh and Ga[39]), indicating strong atomic interactions. The next group of Rh−Ga and Ga−Ga distances is close to the sum of the atomic (metallic) radii. The shortest distances between Eu and Ga are also much shorter compared to the sum of the atomic (metallic) radii (2.04 Å for Eu). A similar behavior of the interatomic distances was observed for the chemically related binary compounds Rh_4Ga_{21}, Rh_3Ga_{16},[40] and $IrGa_2$[41] as well as for the ternary compounds $Eu_2Rh_3Ga_9$ and $Eu_2Ir_3Ga_9$.[26] The fact that an application of different radii systems even as a rough criterion for the systematization of the atomic interactions for $EuTM_2Ga_8$ compounds did not give reliable results was the starting point for analysis of the chemical bonding with quantum chemical methods.

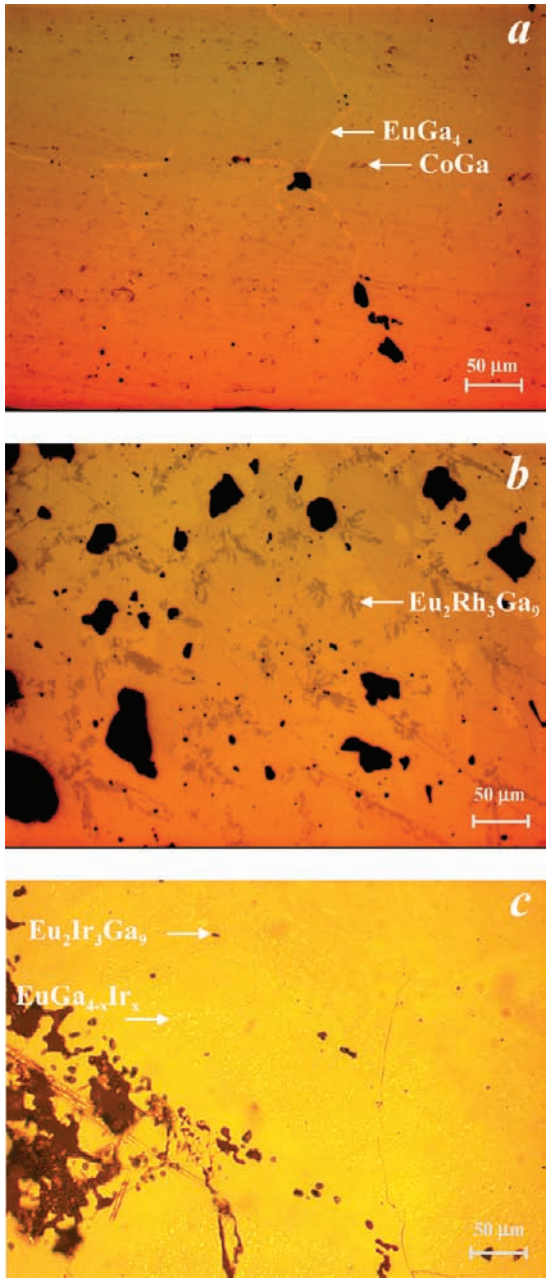

Figure 2. Microstructure of the samples $EuCo_2Ga_8$ (a), $EuRh_2Ga_8$ (b), and $EuIr_2Ga_8$ (c) in polarized light. Besides the differently oriented grains of the majority phases, only traces of minority phases were observed on the grain boundaries.

3.3. Chemical Bonding. Spin-polarized band structure calculations were performed for $EuRh_2Ga_8$ (introducing the spin polarization yielded a decrease of the total energy by ca. 2 Ry). Analysis of the electronic density of states (Figure 4) shows mostly the europium f and, to a very small extent, europium d states being spin polarized, while all other atomic contributions do not reveal noticeable spin polarization. The d states of rhodium are positioned mainly between −6 and −3 eV, with a small contribution to the region above −3 eV, and practically do not contribute to the DOS at the Fermi level. The Ga(s) contributions are visible in the low-energy part of

(39) Emsley, J. *The Elements*; Clarendon Press: Oxford, U.K., **1991**.
(40) Bostrom, M.; Prots, Yu.; Grin, Yu. *J. Solid State Chem.* **2006**, *179*, 2472–2478.
(41) Bostrom, M.; Prots, Yu.; Grin, Yu. *Solid State Sci.* **2004**, *6*, 499–503.

Table 2. Atomic Coordinates and Isotropic Displacement Parameters for $EuTM_2Ga_8$, TM = Co, Rh, Ir[a]

atom	site	*x*	*y*	*z*	B_{iso}	B_{11}	B_{22}	B_{33}	B_{12}
Eu	4*f*	0.6576(2)	0.1808(2)	1/2	0.60(2)	0.52(4)	1.01(4)	0.27(4)	−0.40(9)
		0.6577(2)	0.1811(1)	1/2	0.77(4)	0.79(7)	1.07(7)	0.46(7)	0.07(7)
		0.65657(4)	0.18066(4)	1/2	0.656(9)	0.46(2)	0.94(2)	0.57(2)	−0.08(1)
TM1	4*f*	0.3489(6)	0.0978(3)	1/2	0.61(9)	0.5(2)	0.6(1)	0.7(2)	−0.2(2)
		0.3449(2)	0.0948(2)	1/2	0.48(6)	0.6 (1)	0.12(9)	0.7(1)	0.04(9)
		0.34542(3)	0.09536(2)	1/2	0.254(7)	0.22(1)	0.25(2)	0.29(2)	0.00(1)
TM2	4*f*	0.9674(4)	0.0927(3)	1/2	0.48(8)	0.8(2)	0.4(1)	0.2(2)	−0.4(1)
		0.9650(2)	0.0966(2)	1/2	0.49(6)	0.63(9)	0.56(9)	0.3(1)	−0.05(9)
		0.96513(3)	0.09720(3)	1/2	0.397(8)	0.26(1)	0.34(2)	0.60(2)	0.05(1)
Ga1	2*a*	0	0	0	0.4(1)	0.4(2)	0.4(1)	0.3(2)	0.0(1)
		0	0	0	0.9(1)	1.5(3)	0.8(3)	0.2(3)	0.2(2)
		0	0	0	0.66(3)	0.87(5)	0.56(5)	0.54(6)	0.14(4)
Ga2	2*d*	0	1/2	1/2	0.59(9)	0.3(1)	0.7(1)	0.8(2)	0.0(1)
		0	1/2	1/2	1.4(1)	0.8(2)	1.0(2)	2.5(3)	−0.3(2)
		0	1/2	1/2	1.02(3)	0.63(5)	0.77(5)	1.66(7)	−0.23(4)
Ga3	4*f*	0.1619(5)	0.0455(3)	1/2	0.84(7)	0.6(1)	1.2(1)	0.8(1)	0.0(2)
		0.1602(4)	0.0432(3)	1/2	1.04(9)	0.6(2)	1.2(2)	1.3(2)	−0.5(1)
		0.15962(9)	0.04377(8)	1/2	0.77(2)	0.27(3)	0.79(4)	1.24(4)	−0.16(3)
Ga4	4*f*	0.9026(4)	0.2448(3)	1/2	0.63(6)	0.7(1)	0.5(1)	0.8(1)	−0.01(9)
		0.9018(4)	0.2490(3)	1/2	1.26(9)	1.4(2)	0.5(1)	1.9(2)	0.2(1)
		0.8993(1)	0.24828(8)	1/2	1.05(3)	0.27(3)	0.79(4)	1.24(4)	−0.16(3)
Ga5	4*e*	0.0500(3)	0.1816(3)	0	0.67(7)	0.6(1)	0.8(1)	0.6(1)	−0.1(2)
		0.0505(3)	0.1855(3)	0	0.74(9)	0.7(2)	0.7(1)	0.8(2)	−0.4(1)
		0.05090(8)	0.18525(8)	0	0.55(2)	0.41(3)	0.57(4)	0.66(4)	−0.11(3)
Ga6	4*e*	0.8362(4)	0.1200(2)	0	0.62(8)	0.5(1)	0.4(1)	0.9(2)	0.1 (2)
		0.8340(3)	0.1229(3)	0	0.8(1)	0.5(2)	1.4(2)	0.7(2)	0.1(1)
		0.83233(8)	0.12303(7)	0	0.56(2)	0.30(3)	0.71(4)	0.68(4)	0.00(3)
Ga7	4*e*	0.6703(3)	0.0098(2)	0	0.54(8)	0.4(2)	0.7(1)	0.5(1)	0.1 (1)
		0.6693(3)	0.0140(3)	0	0.82(9)	1.3(2)	0.8(2)	0.4(1)	−0.3(1)
		0.67021(9)	0.01353(7)	0	0.60(2)	0.72(4)	0.48(4)	0.62(4)	−0.16(3)
Ga8	4*e*	0.2615(3)	0.1742(3)	0	0.75(8)	0.8(1)	0.8(1)	0.7(2)	0.1(1)
		0.2588(3)	0.1765(3)	0	0.83(9)	0.9(2)	0.8(1)	0.8(2)	0.3(1)
		0.25794(8)	0.17730(8)	0	0.58(2)	0.35(3)	0.80(4)	0.59(4)	0.21(3)
Ga9	4*e*	0.4756(3)	0.1336(2)	0	0.34(7)	0.3(1)	0.3(1)	0.4(2)	−0.1(1)
		0.4785(3)	0.1327(3)	0	0.48(9)	0.4(2)	0.6(1)	0.5(2)	0.1(1)
		0.47883(8)	0.13310(8)	0	0.56(2)	0.39(3)	0.67(4)	0.62(4)	−0.08(3)

[a] For each position, the first line gives the parameter values for TM = Co; the second - for TM = Rh, and the third - for TM = Ir. Atomic desplacement parameter is defined as $\exp[-1/4\,(B_{11}a^2h^2 + \ldots 2B_{23}bckl)]$. $B_{13} = B_{23} = 0$ for all positions.

the bonding region ($E < -6$ eV). The p states of Ga5−Ga9, which form the first coordination shell around the Eu atoms in the form of a pentagonal prism (cf. the shortest Eu−Ga distances in Table 3), contribute to the DOS below the Fermi level (-3 eV $< E < E_F$) as well as in the intermediate region (-6 eV $< E < -3$ eV), whereas the p contributions of the Ga2−Ga4 atoms, which center the faces of the pentagonal prism, are observed mostly in the intermediate region. The s contributions of the Rh atoms, which form the shortest distances with Ga2−Ga4, are also found predominantly in the intermediate region with long tails to lower energies and toward the Fermi level. This already suggests different interactions of europium and rhodium with the different parts of the gallium environment.

The confirmation of such a bonding picture was obtained by the analysis of the electron localizability indicator in combination with the electron density. The evaluation of the electron density according to the QTAIM method of Bader[38] yielded an atomic basin for each atom. The shapes of the basins for Eu, Rh1, Rh2, Ga1, Ga2, and Ga3 are shown in Figure 5. Integration of the electron density within the atomic basins gives 61.9 electrons (e^-) for Eu, 46.0 e^- for Rh1, 45.9 e^- for Rh2, 30.5 e^- for Ga1, 30.8 e^- for Ga2, 31.0 e^- for Ga3, 30.8 e^- for Ga4, 30.8 e^- for Ga5, 31.0 e^- for Ga6, 30.9 e^- for Ga7, 31.0 e^- for Ga8, and 30.9 e^- for Ga9. In this way, the whole electron density is distributed in the basins centered at the atomic nuclei. The result reflects the charge difference between the interacting atomic volumes. The so-obtained QTAIM charges and the charge transfer giving the ionic charges of +1.1 for Eu, +0.5 to 0 for Ga, and −0.9 to −1.0 for Rh are in agreement with the electronegativity (EN) relation between the components ($EN_{Eu} < EN_{Ga} < EN_{Rh}$).

The bonding situation was further analyzed utilizing the electron localizability indicator. ELI-D for the triplet coupled electrons was computed from the density matrices at the spin-polarized level following eqs. 5 and 37 of ref. 34, though we are aware that in this case the wave function is not an eigenfunction of the spin operator (spin contamination). As will be shown below, the spin contamination in the case of $EuRh_2Ga_8$ is relatively small and does not influence the topology of the function noticeably.

A striking feature of the ELI-D diagram is the spherical regions of high ELI-D values around the atomic nuclei, highlighting the atomic shell structure. Here, it is necessary to mention that, in the ELI-D representation, the shells are composed mainly from the electrons with the main quantum number according to the shell number, but with strong intermixing of the electrons with higher and lower main quantum number, as shown in Figure 6c for the isolated europium atom. The penultimate ELI-D shells of Rh (fourth shell) and Eu (fifth shell), as shown in Figure 6b, are structurized (Eu, strongly; Rh, less); that is, they deviate from the spherical symmetry characteristic for noninteracting isolated atoms. This can be

Table 3. Interatomic Distances (Å) in $EuCo_2Ga_8$, $EuRh_2Ga_8$, and $EuIr_2Ga_8$

$EuCo_2Ga_8$		$EuRh_2Ga_8$		$EuIr_2Ga_8$	
atoms	distance	atoms	distance	atoms	distance
Eu−2Ga9	3.108(3)	Eu−2Ga9	3.138(3)	Eu−2Ga9	3.1345(9)
2Ga6	3.125(4)	2Ga5	3.145(3)	2Ga6	3.1532(9)
2Ga5	3.128(4)	2Ga6	3.146(3)	2Ga5	3.1571(9)
2Ga8	3.177(3)	2Ga8	3.197(3)	2Ga8	3.2093(9)
Ga4	3.181(5)	2Ga7	3.206(3)	2Ga7	3.2197(9)
2Ga7	3.186(3)	Ga4	3.232(5)	Ga4	3.221(1)
Ga2	3.255(2)	Ga2	3.319(2)	Ga2	3.3100(5)
Ga4	3.347(5)	Ga4	3.384(5)	Ga4	3.411(1)
Ga3	3.937(5)	Ga3	4.013(4)	Ga3	4.033(1)
Ga3	3.953(5)	Ga3	4.046(4)	Ga3	4.051(1)
Co1	3.974(6)	Rh1	4.047(3)	Ir1	4.0568(6)
Co1	4.007(5)	Rh1	4.050(3)	Ir2	4.0621(6)
Co1	4.019(7)	Rh2	4.066(3)	Ir1	4.0648(6)
2Eu	4.0378(2)	2Eu	4.1172(2)	2Eu	4.1486(2)
Co1−Ga2	2.347(6)	Rh1−Ga2	2.399(3)	Ir1−Ga4	2.397(1)
Ga4	2.360(6)	Ga4	2.402(5)	Ga2	2.4025(4)
Ga3	2.444(9)	Ga3	2.448(5)	Ga3	2.465(1)
2Ga8	2.542(4)	2Ga7	2.611(3)	2Ga7	2.6272(7)
2Ga7	2.555(3)	2Ga8	2.618(3)	2Ga8	2.6406(7)
2Ga9	2.612(5)	2Ga9	2.716(3)	2Ga9	2.7288(7)
Co2−Ga4	2.332(6)	Rh2−Ga4	2.374(5)	Ir2−Ga4	2.371(1)
2Ga1	2.453(2)	2Ga1	2.538(2)	2Ga1	2.5569(3)
Ga3	2.511(8)	Ga3	2.581(5)	Ga3	2.578(1)
Ga3	2.555(7)	Ga3	2.587(5)	Ga3	2.602(1)
2Ga5	2.601(4)	2Ga5	2.665(3)	2Ga5	2.6739(7)
2Ga6	2.625(5)	2Ga6	2.667(3)	2Ga6	2.6940(7)
Co2	2.786(6)	Rh2	2.969(4)	Ir2	2.9898(5)
Ga1−4Co2	2.453(2)	Ga1−4Rh2	2.538(2)	Ga1−4Ir2	2.5569(3)
2Ga6	2.669(4)	2Ga6	2.763(4)	2Ga6	2.784(1)
2Ga5	2.685(4)	2Ga5	2.796(4)	2Ga5	2.797(1)
4Ga3	2.924(4)	4Ga3	2.952(3)	4Ga3	2.9625(8)
Ga2−2Co1	2.347(6)	Ga2−2Rh1	2.399(3)	Ga2−2Ir1	2.4025(4)
4Ga9	2.803(2)	4Ga9	2.846(3)	4Ga9	2.8637(8)
4Ga7	2.929(3)	4Ga7	2.971(3)	4Ga7	2.9931(8)
2Eu	3.255(2)	2Eu	3.319(2)	2Eu	3.3100(5)
Ga3−Co1	2.444(9)	Ga3−Rh1	2.448(5)	Ga3−Ir1	2.465(1)
Co2	2.511(8)	Rh2	2.581(5)	Ir2	2.578(1)
Co2	2.555(7)	Rh2	2.587(5)	Ir2	2.602(1)
2Ga1	2.924(4)	2Ga1	2.952(3)	2Ga1	2.9625(8)
2Ga8	3.007(5)	2Ga7	3.092(4)	2Ga7	3.103(1)
2Ga7	3.010(5)	2Ga8	3.100(4)	2Ga8	3.114(1)
2Ga6	3.121(4)	2Ga6	3.192(4)	2Ga6	3.213(1)
2Ga5	3.138(5)	2Ga5	3.242(4)	2Ga5	3.242(1)
Ga4−Co2	2.332(6)	Ga4−Rh2	2.374(5)	Ga4−Ir2	2.371(1)
Co1	2.360(6)	Rh1	2.402(5)	Ir1	2.397(1)
2Ga9	2.821(3)	2Ga9	2.862(4)	2Ga9	2.890(1)
2Ga6	2.825(4)	2Ga6	2.896(4)	2Ga6	2.899(1)
2Ga5	2.874(4)	2Ga5	2.935(4)	2Ga8	2.947(8)
2Ga8	2.917(4)	2Ga8	2.946(4)	2Ga5	2.970(1)
Ga5−2Co2	2.814(6)	Ga5−Ga8	2.627(5)	Ga5−Ga8	2.616(2)
Ga8	2.632(5)	2Rh2	2.665(3)	2Ir2	2.6739(7)
Ga1	2.685(4)	Ga1	2.796(4)	Ga1	2.797(1)
Ga6	2.801(6)	Ga9	2.818(5)	Ga9	2.821(2)
Ga9	2.814(5)	Ga6	2.879(5)	Ga6	2.907(2)
2Ga4	2.874(4)	2Ga4	2.935(4)	2Ga4	2.970(1)
Eu	3.128(4)	2Eu	3.145(3)	2Eu	3.1571(9)
2Ga3	3.138(5)	2Ga3	3.242(4)	2Ga3	3.242(1)
Ga6−Ga7	2.601(6)	Ga6−Ga7	2.620(6)	Ga6−Ga7	2.604(2)
2Co2	2.625(5)	2Rh2	2.667(3)	2Ir2	2.6940(7)
Ga1	2.669(4)	Ga1	2.763(4)	Ga1	2.784(1)
Ga5	2.801(6)	Ga5	2.879(5)	2Ga4	2.899(1)
2Ga4	2.825(4)	2Ga4	2.896(4)	Ga5	2.907(2)
Ga8	3.101(5)	Ga8	3.092(5)	Ga8	3.081(2)
2Ga3	3.121(4)	2Eu	3.146(3)	2Eu	3.1532(9)
2Eu	3.125(4)	2Ga3	3.192(4)	2Ga3	3.213(1)
Ga7−2Co1	2.555(3)	Ga7−2Rh1	2.611(3)	Ga7−Ga6	2.604(2)
Ga6	2.601(6)	Ga6	2.620(6)	2Ir1	2.6272(7)
Ga9	2.746(5)	Ga9	2.845(5)	Ga9	2.861(2)
Ga8	2.778(5)	Ga8	2.939(5)	Ga8	2.948(2)
2Ga2	2.929(3)	Ga9	2.969(5)	Ga9	2.987(2)
Ga9	3.005(5)	2Ga2	2.971(3)	2Ga2	2.9931(8)
2Ga3	3.010(5)	2Ga3	3.092(4)	2Ga3	3.103(1)

Table 3. Continued

$EuCo_2Ga_8$		$EuRh_2Ga_8$		$EuIr_2Ga_8$	
atoms	distance	atoms	distance	atoms	distance
2Eu	3.186(3)	2Eu	3.206(3)	2Eu	3.2197(9)
Ga8−2Co1	2.542(4)	Ga8−2Rh1	2.618(3)	Ga8−Ga5	2.616(2)
Ga5	2.632(5)	Ga5	2.627(5)	2Ir1	2.6406(7)
Ga9	2.725(5)	Ga9	2.842(5)	Ga9	2.863(2)
Ga7	2.778(5)	Ga7	2.939(5)	2Ga4	2.947(1)
2Ga4	2.917(4)	2Ga4	2.946(4)	Ga7	2.948(2)
2Ga3	3.007(5)	Ga6	3.092(5)	Ga6	3.081(2)
Ga6	3.101(5)	2Ga3	3.100(4)	2Ga3	3.114(1)
2Eu	3.177(3)	2Eu	3.197(3)	2Eu	3.2093(9)
Ga9−2Co1	2.612(5)	Ga9−2Rh1	2.716(3)	Ga9−2Ir1	2.7288(7)
Ga8	2.725(5)	Ga5	2.818(5)	Ga5	2.821(2)
Ga7	2.746(5)	Ga8	2.842(5)	Ga7	2.861(2)
2Ga2	2.803(2)	Ga7	2.845(5)	Ga8	2.863(2)
Ga5	2.814(5)	2Ga2	2.846(3)	2Ga2	2.8637(8)
2Ga4	2.821(3)	2Ga4	2.862(4)	2Ga4	2.890(1)
Ga7	3.005(5)	Ga7	2.969(5)	Ga7	2.987(2)
2Eu	3.108(3)	2Eu	3.138(3)	2Eu	3.1345(9)

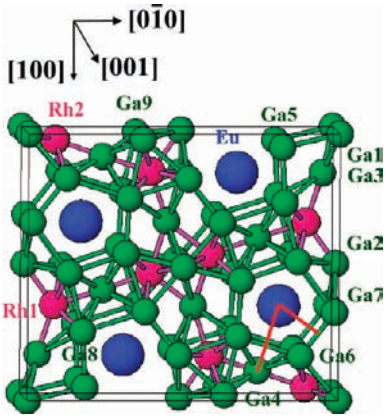

Figure 3. Crystal structure of $EuRh_2Ga_8$ in projection along [001]. The shortest distances Rh−Ga and Ga−Ga are drawn in pink and green, respectively. The red lines describe selected directions for the ELI representation (cf. Figure 8).

quantified with the structuring index ε (the difference between the highest ELI-D value in the examined shell and the ELI-D value at which the localization domain is without a "hole").[42] The respective indexes for ELI-D are ε_Rh = 0.04 (fourth shell, average for two atoms) and ε_Eu = 0.40 (fifth shell), compared with the average ε_Ga = 0.015 for the third shells of Ga atoms. The structuring of the inner ELI-D shells is shown to be an indication for participation of these electrons in the bonding.[42,44] A more detailed analysis of this participation is made below by means of partial ELI-D contributions.

The next relevant topological features are the ELI-D maxima between the Ga atoms forming pentagonal prisms centered by the Eu atoms (Figures 6a,b). They can be seen as a signature of the covalent bonding between the Ga atoms. ELI-D shows in addition attractors in the vicinity of the Rh and Ga atoms. Either ring-shaped localization domains like between Rh1 and Ga3

(42) Wagner, F. R.; Bezugly, V.; Kohout, M.; Grin, Yu. *Chem.—Eur. J.* **2007**, *13*, 5724–5741.
(43) Kohout, M.; Wagner, F. R.; Grin, Yu. *Theor. Chem. Acc.* **2008**, *119*, 413–420.
(44) Kohout, M.; Wagner, F. R.; Grin, Yu. *Theor. Chem. Acc.* **2002**, *108*, 150–156.

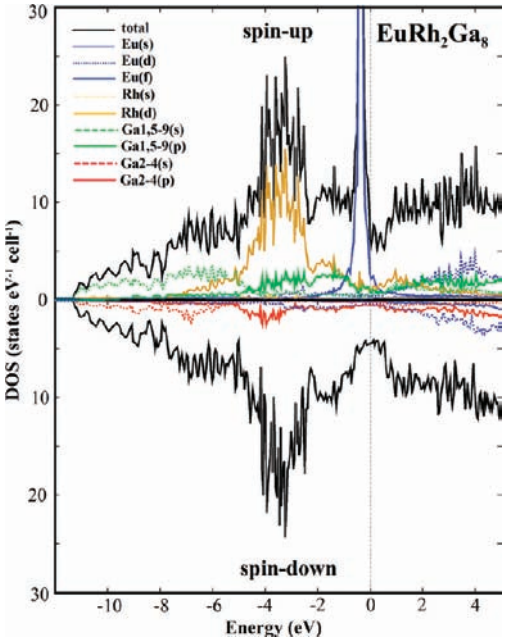

Figure 4. Spin-polarized electronic density of states for $EuRh_2Ga_8$ together with the partial contributions of atomic states. Mainly Eu(f) states show a marked spin polarization. All other contributions are equal in both channels and are shown in different parts of the figure for transparency reasons.

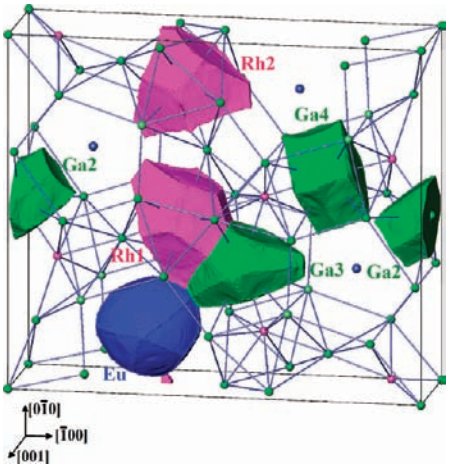

Figure 5. Selected QTAIM atoms in $EuRh_2Ga_8$.

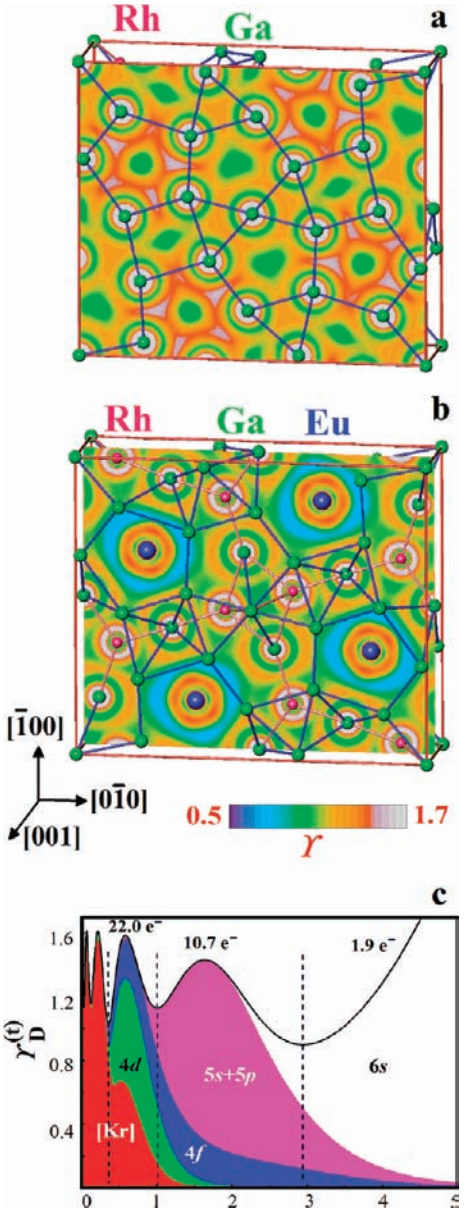

Figure 6. Electron localizability indicator Y in $EuRh_2Ga_8$: (a) ELI map at $z = 0$; (b) ELI map at $z = 0.5$; (c) ELI-D distribution for the free europium atom (spin polarized case). Electron counts for the outer shells are obtained as follows: 6th, 1.6[6s] + 0.2[5s + p] + 0.1[4f]; 5th, 0.3[6s] + 6.8[5s + p] + 0.9[4d] + 2.4[4f].

are observed or the attractors are located within the gallium shell around the rhodium atoms (Figures 6a,b and 7a). The localization domains for these attractors are clearly grouped around the Ga atoms. Additional ELI-D attractors are found between the Ga1 and Ga3 atoms, as well as between the gallium atoms Ga5−Ga9 forming pentagonal prisms. All together, these Rh and Ga atoms form a network polyanion with (possibly) polar covalent bonds. The polar character of these bonds is revealed by the charge transfer between the QTAIM atoms (see above). Participation of the electrons of the fourth shell of rhodium is discussed below by means of the partial ELI-D contributions. Europium species are located in the cavities of the polyanion.

In general, the ELI-D field divides the space into the core basins (first five shells for Eu, four for rhodium, and three for gallium, core basins surround the nuclei) and the valence basins, which is the principal difference if compared to the Bader's analysis of electron density described above. Thus, the electron density is distributed between the core and valence basins. While Bader's analysis gives the total amount and the charge difference between the structural parts, the combined ELI-D/ED analysis allows one to understand how the interaction between the different parts of the crystal structure is spatially organized. The integration of the electron density within the four inner ELI-D shells of the Eu species (atomic core) yields 61.4 electrons. This gives a charge transfer of 1.6 electrons to the Ga−Rh network and reveals the ionic interaction between the europium cation and the $[Rh_2Ga_8]$ polyanion. However, the observed charge transfer is less than the 1.9 electrons in the valence shell, determined from the ELI-D distribution for a free Eu atom (Figure 6c). This, together with the structuring

of the fifth ELI-D shell of Eu in $EuRh_2Ga_8$, points toward the additional bonding interaction between Eu and the Rh−Ga network.

These kinds of interactions can be further analyzed by partial ELI-D contributions. ELI-D can be seen, in a simplistic way, as a product between the charge needed to form a fixed fraction of an electron pair and the volume demanded by that pair fraction (so-called pair-volume function).[43] Now, the charge can be decomposed into contributions, for instance, from states belonging to a certain energy range in the electronic DOS (Figure 4). The product of such contributions and the associated pair-volume function yields the contribution of the particular energy range to the total ELI-D, the so-called partial ELI-D.[42,45] Of course, in this representation, the sum of all partial ELI-D contributions yields the total ELI-D, the same way that the sum of all partial electron density contributions must result in the total electron density. Thus, such a decomposition of ELI-D into contributions is exact and consistent (in contrast to a decomposition of the electron localization function ELF into valence-core, sigma-pi, etc. contributions).

For the analysis, the contributions from three different regions were computed, -11 eV $\leq E \leq -5$ eV, -5 eV $\leq E \leq -1$ eV, and -1 eV $\leq E \leq E_F$ (cf. electronic DOS in Figure 4). The results of the calculations are shown in Figure 7. A particular isosurface of the triplet ELI-D (single representation of both spin channels) with $Y_D^{(t)} = 1.04$ is used for visualization of the ELI-D topology in $EuRh_2Ga_8$ (positions of the attractors in the valence region and within the inner shells). The coloring of the isosurface reflects the contribution of the according energy range in the electronic DOS to the triplet ELI-D at the given position. The states from the lowest (valence) energy range (contributions of Ga atomic states) participate in ELI-D mainly (around 50%) in the region between Ga1 and Ga3 as well as in the outer regions of the Ga prisms (Figure 7d). The partial ELI-D contributions from the second energy range (atomic Rh(d) and Ga(p) levels) shows that the ELI-D maxima between Rh and Ga are, to a large extent, due to the interaction between these atomic levels (around 50% participation, Figure 7c). The partial ELI-D computed from the states with the highest energy range (1 eV below Fermi level) nicely shows that the structuring of the fifth Eu shell is due to the f states. In addition, it reveals the clear participation of the Eu(f) states in the bonding interaction toward the Rh or Ga atoms of the equatorial ring of the coordination sphere of Eu (Figure 7b).

For two particular directions in the structure (Figure 8a), the contributions of different energy ranges in DOS are analyzed more in detail. The first direction is along the line connecting Eu with the middle point of the Ga6−Ga7 bond, which forms one of the edges of the pentagonal prism around Eu. Another one is the line connecting Eu and Ga4. This line crosses the middle point of the side face of the pentagonal prism formed by four gallium atoms and centered by Ga4 in the equatorial plane of the prism. Both the Ga6−Ga7 bond and the Ga-centered prism's side face are parts of the $[Rh_2Ga_8]$ polyanion. Thus, both lines visualize the interaction between Eu and the $[Rh_2Ga_8]$ polyanion. In both cases, the contributions of the highest energy range of the DOS to the ELI-D in the bonding region are remarkably large. In the case of the equatorial plane of the prism (Eu−Ga4 line), the contribution is around 17% (Figure 8c), larger than in the case of the prism edge (12%, line Eu-to-attractor Ga6−Ga7, Figure 8b).

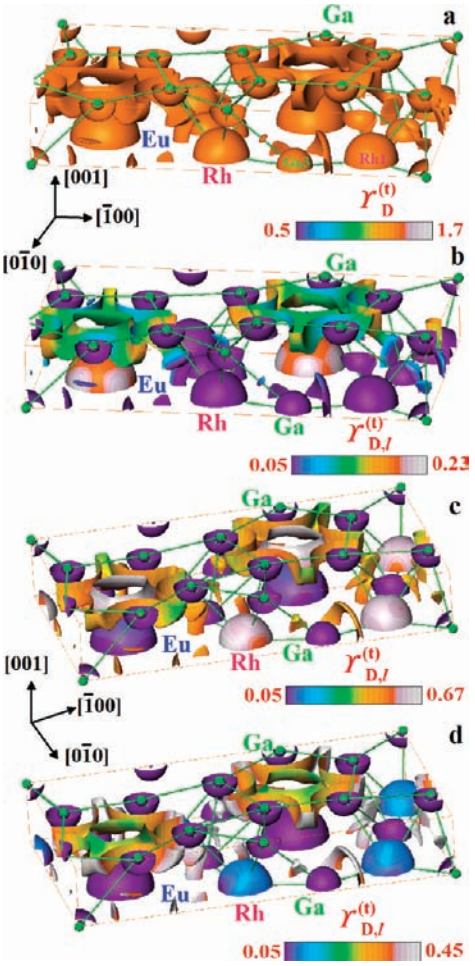

Figure 7. Isosurface of the triplet ELI-D ($Y_D^{(t)} = 1.04$). (a) Colored with the partial ELI-D calculated for the different energy intervals in electronic DOS (cf. Figure 3). (b) -1 eV $< E \leq E_F$ (mostly Eu(f) and minor Ga1,5−9(p) states. (c) -5 eV $< E \leq -1$ eV (Rh(d) and Ga1,5−9(p) states. (d) -11 eV $< E \leq -5$ eV (mostly Ga(s), minor Rh(*s*,d) and Ga2−4(p) states). Only a 1/4 of the unit cell is shown ($0 \leq x \leq 1$, $0 \leq y \leq 0.5$; $0 \leq z \leq 0.5$).

In total, chemical bonding in $EuRh_2Ga_8$ may be described by the formation of a $[Rh_2Ga_8]$ polyanion by Ga−Ga and polar Ga−Rh bonds. Europium shows two types of interactions with the polyanion: one is more of an ionic nature with the charge transfer from europium to the Ga−Ga bonds in the first coordination shell; the second one is a directed one caused by participation of the electrons of the fifth shell of europium in the bonding (mainly in the equatorial plane of the pentagonal prism). The second interaction may cause the appearance of the $4f^6$ channel and intermediate valence of europium observed in the XAS experiments.

3.4. Electronic State of Europium. The bonding picture above finds its indirect confirmation in the magnetic

(45) Dashjav, E.; Prots, Yu.; Kreiner, G.; Schnelle, W.; Wagner, F. R.; Kniep, R. *J. Solid State Chem.* **2008**, *181*, 3121–3129.

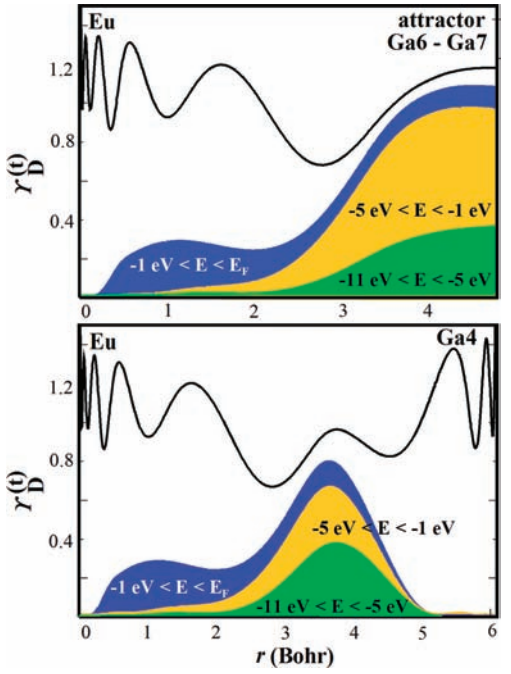

Figure 8. Contributions of different DOS regions (cf. Figure 4, spin-up) to the ELI-D: (top) pELI-D contributions on the line between Eu and Ga5−Ga6 bonding attractor (cf. Figure 3); (bottom) pELI-D contributions on the line between Eu and Ga4 (cf. Figure 3). Black line, total ELI-D; color fields, partial ELI-D for different energy regions in electronic DOS.

behavior of the Eu{Co,Rh,Ir}$_2$Ga$_8$ compounds. The inverse magnetic susceptibilities $1/\chi = H/M$ of the compounds are plotted in Figure 9 (top). For temperatures above 40 K, the data are well described by the Curie−Weiss law. Fits in the temperature range 40−400 K and $\mu_0 H = 1$ T yield the following parameters: for EuCo$_2$Ga$_8$, the paramagnetic effective moment is $\mu_{eff} = 7.81\ \mu_B$/f.u. and the Weiss temperature $\Theta = -2.0$ K; for EuRh$_2$Ga$_8$, $\mu_{eff} = 8.04\ \mu_B$/f.u. and $\Theta = -5.5$ K; for EuIr$_2$Ga$_8$, $\mu_{eff} = 8.27\ \mu_B$/f.u. and $\Theta = -3.0$ K. While the effective magnetic moment of the Rh compound is only slightly larger than the free ion value of 7.93 μ_B for europium in the $^8S_{7/2}$ ground multiplet of the 4f^7 electronic configuration (Eu^{2+}), the values for the Co compound are significantly smaller, and those for the Ir compound are significantly larger. Small negative Weiss temperatures hint at predominantly antiferromagnetic interaction of the Eu moments.

The magnetic susceptibilities $\chi(T)$ in a low field of $\mu_0 H = 0.01$ T and for $T < 35$ K are depicted in Figure 9 (bottom). Sharp cusps at 20.0(2), 19.5(4), and 15.9(4) K indicate antiferromagnetic long-range ordering of the Eu moments in the Co, Rh, and Ir compounds. For the Rh compound, further anomalies are visible at 12.5(5) and 5.5(3) K, which probably indicate a reordering of the structure of Eu moments. Isothermal magnetization measurements at 1.8 K show a gradual increase of M with H to 4.0 μ_B (EuCo$_2$Ga$_8$), 3.5 μ_B (EuRh$_2$Ga$_8$), and 5.0 μ_B (EuIr$_2$Ga$_8$) at $\mu_0 H = 7$ T and no saturation at high fields. For fields between 2 and 4 T, weak and broad nonhysteretic metamagnetic transitions are seen for all three compounds.

X-ray absorption spectra of EuCo$_2$Ga$_8$, EuRh$_2$Ga$_8$, and EuIr$_2$Ga$_8$ are quite similar (Figure 10). They are

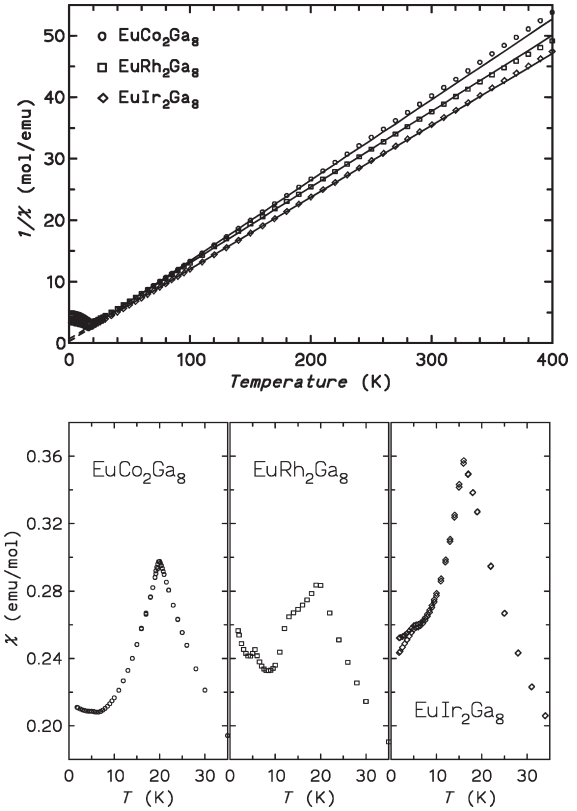

Figure 9. Magnetic behavior of EuTM$_2$Ga$_8$. Inverse magnetic susceptibility $1/\chi = H/M$ of EuTM$_2$Ga$_8$ in a field $\mu_0 H = 1$ T (top). The lines are fits with the Curie−Weiss law; the dashed lines, the extrapolation to low temperatures. (bottom) $\chi(T)$ data (taken in warming after cooling in field) for $\mu_0 H = 0.01$ T showing the antiferromagnetic ordering anomalies.

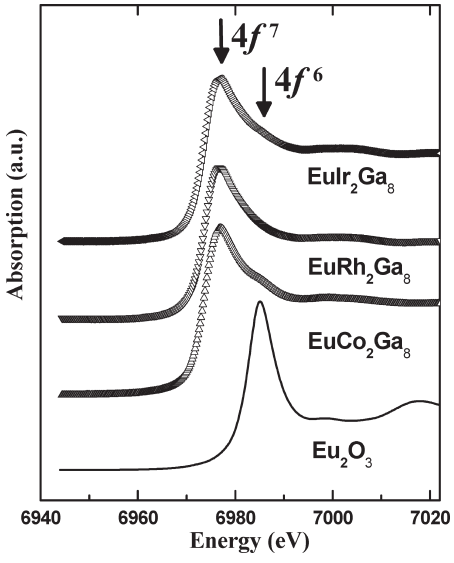

Figure 10. X-ray absorption spectra of EuTM$_2$Ga$_8$ compounds.

dominated by the main signal at ≈6977 eV. This value is, by ≈8 eV, smaller than that observed for the reference compound Eu$_2$O$_3$ (electronic configuration 4f^6, Eu^{3+}) and is characteristic of the 4f^7 electronic configuration. In addition, in each spectrum, a small shoulder is observed on the high-energy side at ≈6983−6884 eV (most visible in EuCo$_2$Ga$_8$), indicating the presence of small admixtures of Eu in the 4f^6 configuration. The signature of both electronic configurations of europium (4f^7 (Eu^{2+}) and 4f^6

(Eu^{3+})) in the investigated samples of $EuTM_2Ga_8$ cannot be explained by impurities, because the minority phases $EuGa_4$, $Eu_2Rh_3Ga_9$, and $Eu_2Ir_3Ga_9$ present in the samples (cf. Figure 2) either do not contain Eu in the $4f^6$ configuration ($EuGa_4$) or show it as an admixture ($Eu_2TM_3Ga_9$).[26] The samples during the experiment were protected against oxidation within a special sample holder (cf. Experimental Section). In addition, no proof of the oxidation of the sample during the XAS experiment was found by powder X-ray diffraction or, especially, by the metallographic analysis, which is much more suitable and sensitive for the amorphous impurities. One of the possible oxidation products may be Eu_3O_4. In this case, its antiferromagnetic ordering should be observed at 5 K. An anomaly in this region is observed at different temperatures in the three materials, which excludes the origin of this feature from Eu_3O_4 (cf. Figure 9 bottom). Neither was EuO (T_N = 71 K) detected in the magnetic susceptibility in the low field (100 Oe). Under the circumstances above, the final decision about the origin of the $4f^6$ configuration of Eu in $EuTM_2Ga_8$ cannot be made. If this feature would be assumed as the intrinsic property of the $EuTM_2Ga_8$ compounds, it would yield an average valence for Eu of ν = 2.14 for $EuCo_2Ga_8$, ν = 2.09 for $EuRh_2Ga_8$, and ν = 2.11 for $EuIr_2Ga_8$. This observation may open an interesting link to the findings of two types of interactions between europium and the Rh−Ga polyanion in bonding analysis.

Conclusions

The isotypic compounds $EuTM_2Ga_8$ (TM = Co, Rh, Ir, crystal structure of the $CeFe_2Al_8$ type) were prepared in order to investigate the chemical interaction between the rare earth metals and their environment in the ternary intermetallic compounds and the influence of the environment of the valence state of the R component. Analysis of the electron localizability indicator revealed formation of a 3D rhodium-gallium polyanion [Rh_2Ga_8]. Europium species are located in the cavities of the polyanion and show two types of interaction: ionic through the charge transfer from the sixth shell and, additionally, covalent by means of the electrons of the fifth shell. Magnetic susceptibility measurements show paramagnetic behavior above 20 K with effective magnetic moments close to the free ion value for Eu^{2+} ($4f^7$). In agreement with the bonding analysis for $EuRh_2Ga_8$, magnetic behavior and X-ray absorption spectra confirm mainly the $4f^7$ with a small admixture of $4f^6$ electronic configuration of europium. If this observation would be assumed as the intrinsic property of the $EuTM_2Ga_8$ compounds, it may open an interesting link to the findings of two types of interactions between europium and TM−Ga polyanion in bonding analysis.

Acknowledgment. The authors thank Mrs. M. Eckert for EDXS measurements, Mrs. S. Muller for thermal analysis, and Mrs. U. Schmidt for chemical analysis. O.S. is indebted to the Max-Planck-Gesellschaft for the research fellowship.